

Evaluation of ASTER Images for Characterization and Mapping of Volcanic Rocks (Basalts)

Paulo Roberto Markoski and Silvia Beatriz Alves Rolim

CEPSRM/UFRGS, Centro Estadual De Pesquisas em Sensoriamento Remoto e Meteorologia – Federal University of Rio Grande do Sul State, Brazil

Correspondence should be addressed to Silvia Beatriz Alves Rolim, silvia.rolim@ufrgs.br

Publication Date: 14 March 2014

Article Link: <http://technical.cloud-journals.com/index.php/IJARSG/article/view/Tech-222>



Copyright © 2014 Paulo Roberto Markoski and Silvia Beatriz Alves Rolim. This is an open access article distributed under the **Creative Commons Attribution License**, which permits unrestricted use, distribution, and reproduction in any medium, provided the original work is properly cited.

Guest Editor-in-Chief: **Dr. Maurício Roberto Veronez**

(This article belongs to the Special Issue “Application of Geotechnology in Urban Planning”)

Abstract The objective of this work was to evaluate the potential of hyperspectral classification techniques in the Advanced Spaceborne Thermal Emission and Reflection Radiometer (ASTER) reflectance data (visible to short wave infrared region) and spatial resolution (15 and 30 m), to map volcanic rocks in Ametista do Sul Region, Rio Grande do Sul State, Brazil. This region is one of the most important amethyst mineralization of the World. The spectral behavior of these rocks is similar to shadows and soils when interpreted with traditional digital classification techniques and multispectral sensors, like TM-Landsat, CCD-CBERS, etc. As an alternative was applied hyperspectral image processing technique (Spectral Angle Mapper - SAM) to identify and discriminate basalt rocks occurrence in mixed pixels. Due to vegetation around and covering some outcrops and the pixel spatial resolution, it was not possible to extract a basalt endmember directly into the ASTER image, being used so an endmember from NASA spectral library. To compare SAM results with traditional classification techniques were applied the Maximum Likelihood (MaxVer) algorithm. The SAM technique produced better results than MaxVer, but the error persisted, even in a lesser proportion, in mixed pixels with “Shadows”, “Soils” and “Basalt” classes.

Keywords *Classification Methods; MaxVer; SAM; Spectral Analysis*

1. Introduction

The Remote Sensing and auxiliary computing techniques are important tools used for identification, geological mapping and mineral exploration. These tools aim the spectral discrimination of targets. To accomplish this discrimination is important to know about the spectral behavior through the observation of diagnostic features that express the physical and chemical composition of each target. One way to perform this study is to use orbital sensors that allow working with an adequate spatial and spectral scale.

It's difficult to perform a digital classification closer of the scene reality because the radiance recorded by a sensor may be a result of the mixture of many materials inside the pixel, added by the atmospheric scattering.

The radiance recorded by a sensor in a pixel may be a mixture of many materials, hampering a digital classification closer the scene reality. Traditional classification methods, such as MaxVer and Minimum Distance [26], use to be applied by prior knowledge of the targets by collecting training samples. Spectral classification methods are also applied by a prior knowledge of the targets, but implying a supervised classification based on sampling and analysis of spectral signatures and their comparison with the image pixels spectra. Such signatures can be obtained collecting *endmembers* (defined as spectrally "pure" features) on the image, measuring in laboratories or field with a spectroradiometer, or searching in spectral libraries. The classification by spectral analysis allows decompose each pixel by its correlation with the material that composes it (spectrum) in a direct way, establishing location and, sometimes, sub-pixel composition [30].

In this context, this study aims to evaluate the potential of hyperspectral classification techniques in the Advanced Spaceborne Thermal Emission and Reflection Radiometer (ASTER) [1] images to map and identify volcanic rocks extracted from amethyst mines in Ametista do Sul region, north of Rio Grande do Sul State, Brazil (Figure 1.1).

The basalt rock is very dark, compact, sometimes with cavities and some crystals developed on the solid mass formed by minerals rich in iron and magnesium. It is a basic igneous rock composed mainly of fine grains of plagioclase feldspar enriched with calcium and pyroxene. Some others minerals such as olivine, magnetite and apatite can be present in the rock.

1.1. Study Area

The study area is located in north of Rio Grande do Sul State, Brazil, City of Ametista do Sul (Figure 1.1). This region is the largest amethyst producer in the world.

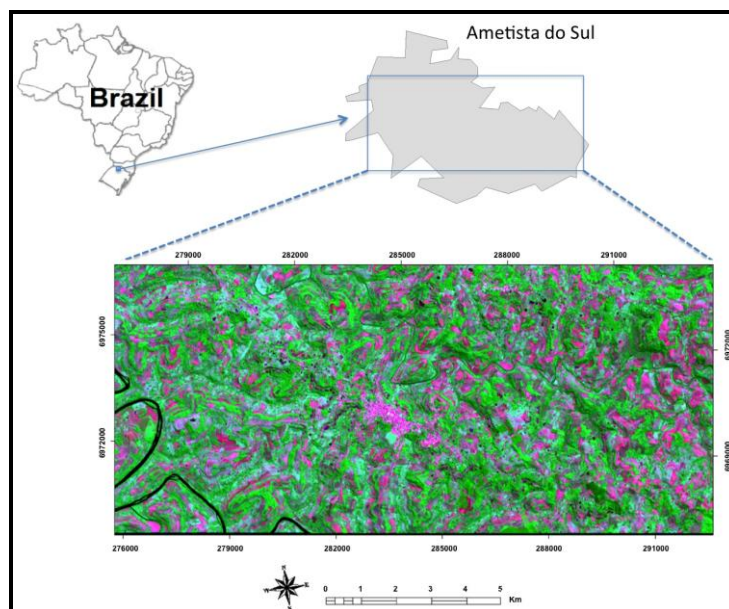


Figure 1.1: Study Area

The basalt is extracted into the mountain during de mining process and deposited outside, where large stacking of rocks is formed (Figure 1.2). These stacks are many times smaller than ASTER pixel size

(VNIR - 15 meters and SWIR – 30 meters). Thus, the pixel composition becomes a mixing of materials, hampering its identification and mapping.



Figure 1.2: Photos of Amethyst Mining Residues/Basalt

2. Mapping Methods

2.1. Traditional Method: MaxVer Algorithm

MaxVer or Maximum Likelihood is a statistical classification method that considers the weighting of the distances between averages classes values using statistical parameters. To be accurate enough, MaxVer needs a number of "pixels" for each training group (more than 30). The training groups define the classes scatter diagram and their probability distributions, considering the normal probability distribution for each training class [7]. The classification limits are defined from points of same classification probability for all classes. This classification method assumes that the user knows previously the analyzed area and the distribution of the classes. In this way, when performed the classification, selection of training samples can be as efficient as possible [7]. The Equation (1) defines the Maximum Likelihood algorithm:

$$g_j(x) = -\frac{1}{2}(x - m_j)^T \Sigma_j^{-1}(x - m_j) - \frac{1}{2} \ln \left| \Sigma_j \right| + \ln P(\omega_j) \quad (1)$$

Where:

m=Vector of means

Σ = Covariance matrix

ω = Occurrence probability of each class

This is the traditional method most commonly used to obtain informational classes from remote sensing images. The spectral distribution of land use classes is considered to be Gaussian or normal, i.e., objects belonging to the same class will present spectral response close to the average values for that class. To obtain satisfactory results is necessary to choose a fairly large number of pixels for each training sample class, and these present a statistical distribution close to the normal distribution [7].

Another important factor to effectiveness results is to obtain a reasonably accurate estimate of the mean vector and covariance matrix for entire spectral class, which also depends the number of pixels included in the training samples [28].

2.2. Spectral Method: Spectral Angle Mapper (SAM)

The spectral classification methods were originally developed for hyperspectral data. The process of image acquisition in contiguous bands allows deriving a spectral reflectance curve, named "imaging spectroscopy" and "Hyperspectral remote sensing" [29]. The goal of imaging spectroscopy is quantitatively measure the spectral signature of the components of the Earth system from calibrated spectra, acquired from images, useful in scientific research and remote sensing applications [22].

This spectral classifications method has provided satisfactory results not only in its application to hyperspectral data, but also in data obtained by multispectral sensors like ASTER [27; 11; 8; 22].

The spectral classification methods can be divided in total pixel detection and sub-pixel scale. The total pixel detection is restricted to map the distribution of the material in its percentage prevalence into the pixel; otherwise it will not be detected. Examples of these classification techniques: Binary Encoding [14]; Tricorder / Tetracorder and its variation Spectral Feature Fitting - SFF [6] and Spectral Angle Mapper - SAM [20]. Mapping sub-pixel scale, the feature is not mapped by predominance into the pixel, but for its occurrence, even small. It is established, hence, a relative estimation of abundance, distribution and occurrence of the target material component, outlining a mixture of materials inside each pixel, expressed in their spectral behavior. Examples of techniques associated with this concept: Linear Spectral Unmixing - LSU [25] Matched Filtering and Mixture Tuned Matched Filtering - MTF [5; 2; 17].

The SAM technique [20] allows fast mapping of the similarity between the pixel spectra and the reference spectra. The reference spectra can be extracted in laboratory, field or extracted from the image. This method assumes that the image data was converted to surface reflectance. The algorithm determines the spectral similarity between two spectra calculating the angle formed between them, treating them as vectors in a space of dimensionality corresponding to the number of bands (nb) (Equation 2).

$$\theta = \cos^{-1} \left[\frac{\sum_{i=1}^n t_i r_i}{\sqrt{\sum_{i=1}^n t_i^2 \sum_{i=1}^n r_i^2}} \right] \quad (2)$$

Where:

n = number of spectral bands

t = reflectance of the pixel spectra

r = reflectance of the reference spectra

This similarity measured is insensitive to gain factors because the angle between two vectors is invariant in relation to the vectors lengths. Laboratory spectra can be directly compared to pixels reflectance spectra, which inherently have a gain factor related to unknown illumination effects due to topography [20]. As a result, a classified image is created, showing the best fit for each pixel, subject to a limit specified by the user. Additionally, "rule" images are provided showing the angular distance (in radians) between each spectra image and each reference spectra. The black pixels in the "rule" image present low spectral angles values, and therefore more similar to the spectra of *end members*. For best viewing, these images are inverted and the smaller angles appear in a clear tone.

3. Method

In this paper were evaluated two classification techniques: algorithm MaxVer and the SAM technique. The reason why were chosen these two techniques is the fact that they have been successfully used in other studies of soil and rocks and the possibility to compare different classification approaches:

traditional classification methods (MaxVer) versus spectral Methods (SAM). An ASTER image, Level 1B (Figure 1.3) was used to test and perform the techniques. A total of 16 points of volcanic rocks exposition area was collected to check the classification/mapping accuracy (Figure 1.3).

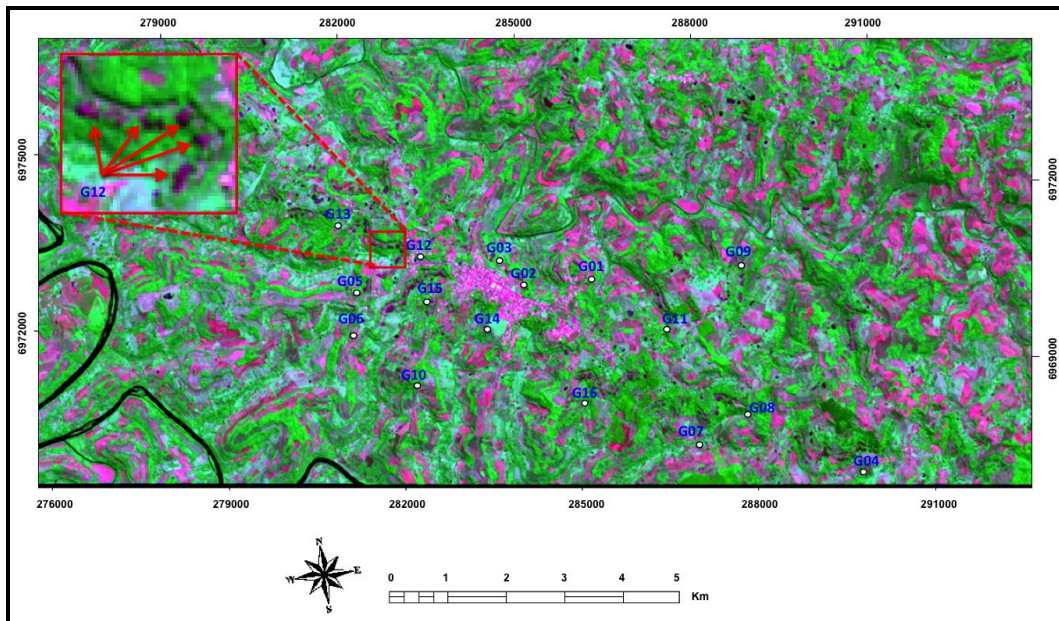


Figure 1.3: Aster Color Composition R (2), G (3), B (1) with the Amethyst Mining Points Distribution, Collected by GPS

3.1. Image Processing

To perform both classifications methods an ASTER Level 1B image was employed. First, the image was submitted to crosstalk effect correction through the software Crosstalk [10]. This problem affect the dispersion of the incident light in the band 4, which is reflected on the focal plane of SWIR bands, producing, for example, appearance of "ghosts" at the interface between land and water surfaces [18]. After that, a SWIR bands spatial re-sampling was performed, artificially, increasing its resolution to 15 m, thus, allowing the composition with VNIR bands in an image database with nine spectral bands. This data set were submitted to atmospheric correction through the Atmospheric Moderate Resolution Radiance and Transmittance Model (MODTRAN), implemented on the algorithm Fast Line-of-sight Atmospheric Analysis of Spectral Hypercube (FLAASH) and converted to apparent reflectance. FLAASH is a first-principles atmospheric correction tool that corrects wavelengths in the visible through near-infrared and shortwave infrared regions, up to 3 μm [9].

FLAASH starts from a standard equation for spectral radiance at a sensor pixel, L , that applies to the solar wavelength range (thermal emission is neglected) and flat, Lambertian materials or their equivalents. The equation is as follows:

$$L = \left(\frac{A\rho}{1 - \rho_{\epsilon}S} \right) + \left(\frac{B\rho_{\epsilon}}{1 - \rho_{\epsilon}S} \right) + L_{\alpha} \quad (3)$$

Where:

ρ is the pixel surface reflectance

ρ_{ϵ} is an average surface reflectance for the pixel and a surrounding region

S is the spherical albedo of the atmosphere

L_{α} is the radiance back scattered by the atmosphere

A and B are coefficients that depend on atmospheric and geometric conditions but not on the surface. Each of these variables depends on the spectral channel; the wavelength index has been omitted for simplicity. The first term in Equation (3) corresponds to radiance that is reflected from the surface and travels directly into the sensor, while the second term corresponds to radiance from the surface that is scattered by the atmosphere into the sensor. The distinction between ρ and ρ_s accounts for the adjacency effect (spatial mixing of radiance among nearby pixels) caused by atmospheric scattering. To ignore the adjacency effect correction, set $\rho_s = \rho$. However, this correction can result in significant reflectance errors at short wavelengths, especially under hazy conditions and when strong contrasts occur among the materials in the scene [9].

The values of A , B , S and L_a are determined from MODTRAN4 calculations that use the viewing and solar angles and the mean surface elevation of the measurement, and they assume a certain model atmosphere, aerosol type, and visible range. The values of A , B , S and L_a are strongly dependent on the water vapor column a27, which is generally not well known and may vary across the scene. To account for unknown and variable column water vapor, the MODTRAN4 calculations are looped over a series of different column amounts, and then selected wavelength channels of the image are analyzed to retrieve estimated amounts for each pixel. Specifically, radiance averages are gathered for two sets of channels: an absorption set centered at a water band (typically 1130 nm) and a reference set of channels taken from just outside the band. A lookup table for retrieving the water vapor from these radiances is constructed [9].

For images that do not contain bands in the appropriate wavelength positions to support water retrieval (for example, Landsat or SPOT), the column water vapor influence is determined by the user-selected atmospheric model. After the water retrieval is performed, Equation (3) is solved for the pixel surface reflectance in all of the sensor channels. The solution method involves computing a spatially averaged radiance image L_s , from which the spatially averaged reflectance ρ_s is estimated using the approximate equation:

$$L_s = \left(\frac{(A + B)\rho_s}{1 - \rho_s S} \right) + L_a \quad (4)$$

Spatial averaging is performed using a point-spread function that describes the relative contributions to the pixel radiance from points on the ground at different distances from the direct line of sight. For accurate results, cloud-containing pixels must be removed prior to averaging. The cloudy pixels are found using a combination of brightness, band ratio, and water vapor tests, as described by [23].

To perform the atmospheric correction in this work, the following image conditions were considered:

- a) Elevation of study area (550 m);
- b) Aerosol levels (visibility: 40 km, rural model). In the Initial Visibility field, is used an estimate of the scene visibility in kilometers (40 to 100 km for clear conditions; 20 to 30 km for moderate haze and 15 km or less for thick haze). Rural model represents aerosols in areas not strongly affected by urban or industrial sources.
- c) Atmospheric model (Mid-Latitude Summer). For the best results, must be select a model whose standard column water vapor a27 is similar to, or somewhat greater than, that expected for the scene.

If no water vapor information is available, the model may be selected based on a seasonal-latitude surface described by [9].

After the atmospheric correction, the classification was performed using the MaxVer algorithm. Were selected six classes: Soil 1, Soil 2, Native Forest, Agriculture, Basalt and Shadow. The interest classes for this work are Shadow, Soils and Basalt. The others were used only to improve the classifier accuracy. For each class were selected a number of pixels greater than 30. After the image classified, geometric correction was performed to compare with the basalt points collected in field.

The following processes were performed to SAM Technique. Due to the small size of the areas with basalt exposition (usually less than one pixel - 15m ASTER), the spectral signature of reference (endmember) cannot be extracted in the ASTER image. As Basalt endmember was employed a spectral signature from the Jonh Hopkins University Spectral Library, available in: <http://speclib.jpl.nasa.gov>. Before processing the SAM technique, the spectral signature was resampled to nine bands ASTER VNIR/SWIR subsystems resolutions (Figure 3.1). A similarity angle of 0.05 radians was used to perform the technique.

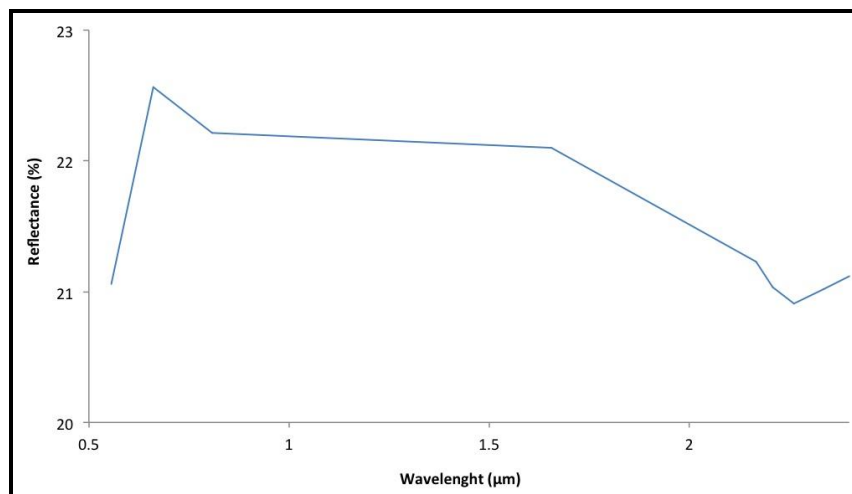


Figure 3.1: Reflectance Spectra of Basalt endmember Extracted from Jonh Hopknis University Spectral Library and Resampled to ASTER VNIR/SWIR Resolution

4. Results

4.1. MaxVer Processing

The ASTER image was classified into six classes: Soil 1, Soil 2, Native Forest, Agriculture, Basalt and Shadow. Figure 4.1 presents the classification results.

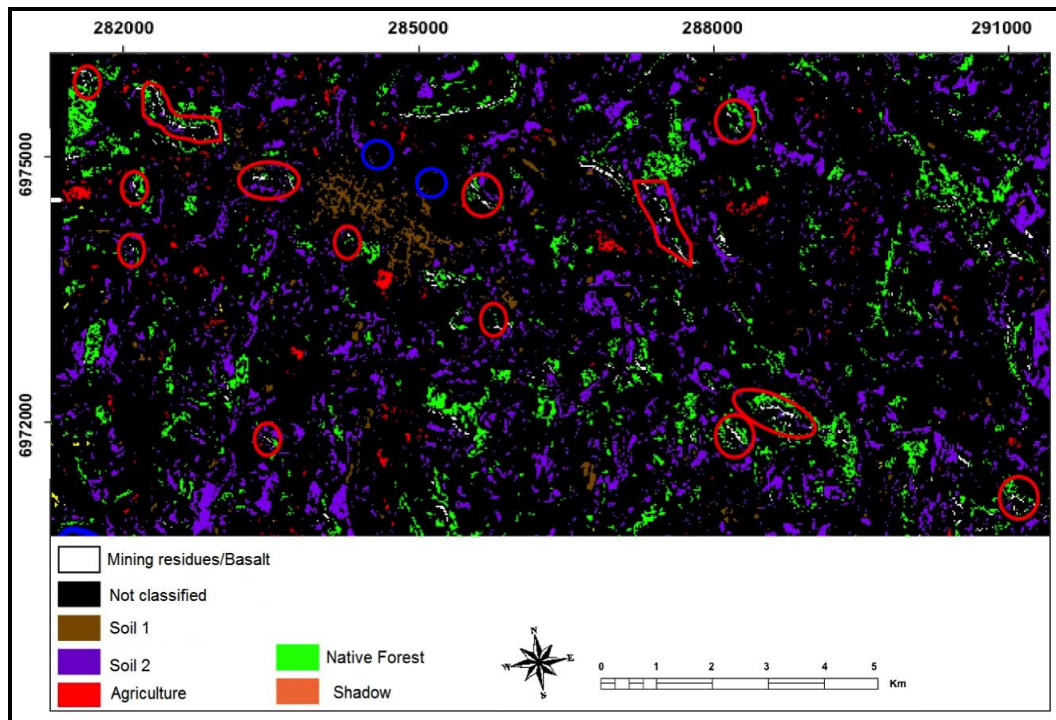


Figure 4.1: MaxVer Classification Results

The MaxVer algorithm classified correctly fourteen of sixteen basalt points (G02 and G03 not classified - blue circles). There is a large occurrence of vegetation closer the mines/basalt, especially native forest, hampering the classification. Due to shaded areas in the visible region, is easily confused with the basalt. These two points were not classified, presumably because they were located in very small mines, where the stacks of basalt are smaller, being strongly influenced by other targets reflectance, such as bare soil or shadow. The main problem found with MaxVer algorithm was the mixture produced between "shadow" "Soils and "basalt" classes. Several shaded areas were classified as "basalt" even when have no occurrence of them. This can be seen in Figure 4.2. In the classification result, the "Shadow" class included several pixels classified as basalt (white color).

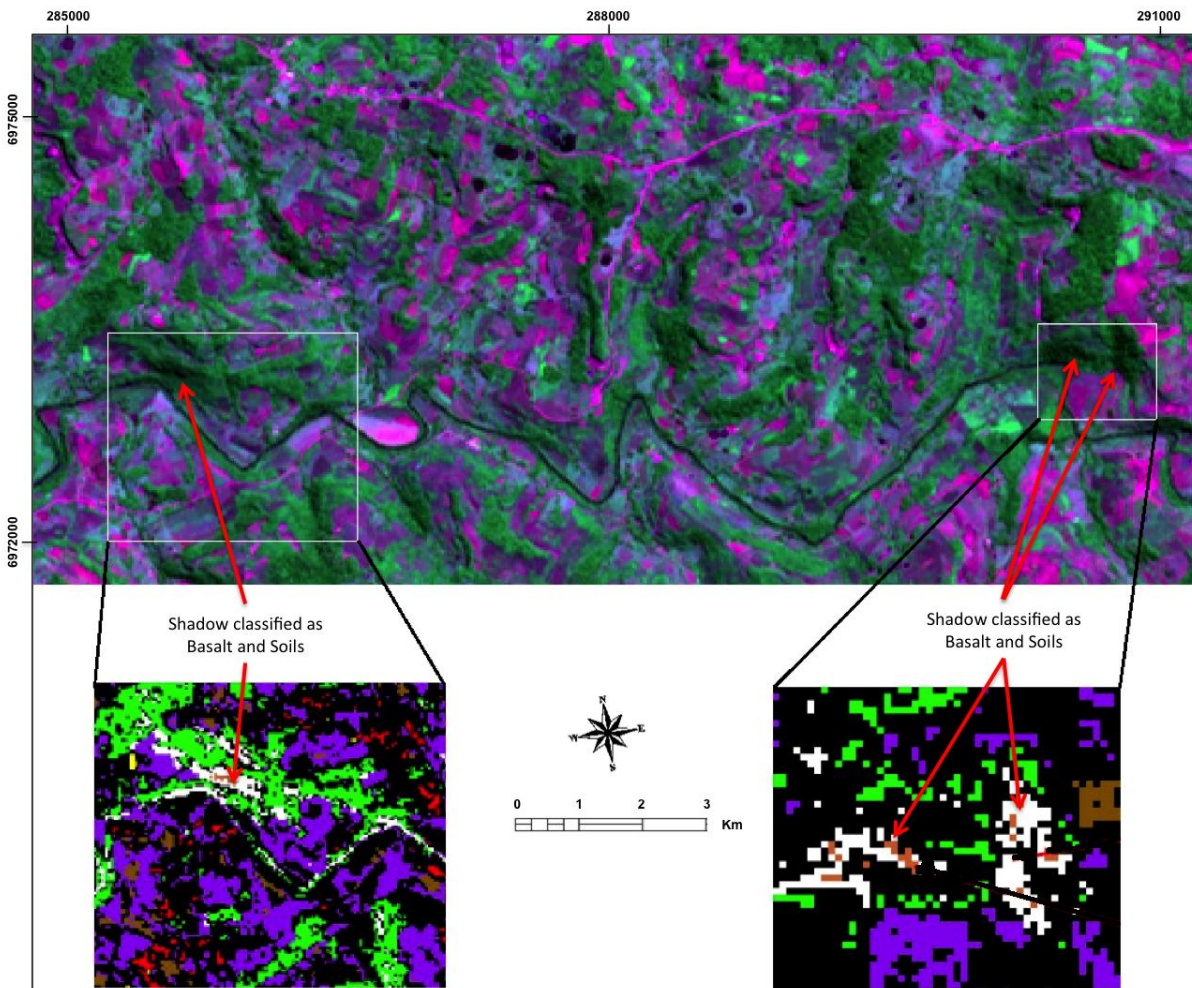


Figure 4.2: Misclassification between “Soils”, “Shadow” and “Basalt” Classes. Shadow Pixels were classified as Basalt and Soils

4.2. SAM Processing

The result of SAM technique processing is presented in Figure 4.3 (rule image). The lighter pixels are those with greatest similarity with the basalt spectral signature, that is, the clearer, more likely to be a pure pixel class.

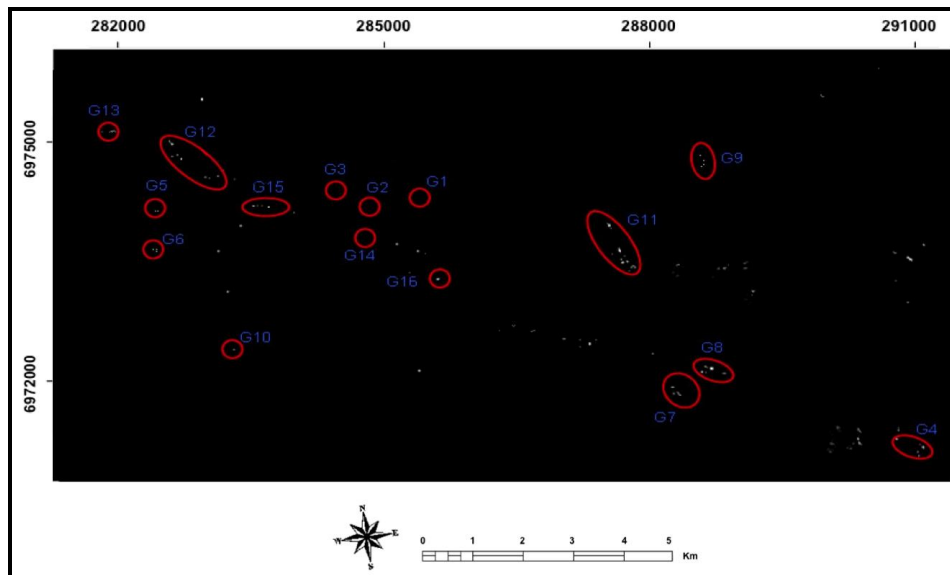


Figure 4.3: SAM Result

The basalt points G1, G2, G3 and G14 did not show similarity with the spectral *endmember* mainly due to the reduced amount of basalt present at these areas, smaller than one pixel (15 m – VNIR, 30 m - SWIR). Most of the polygons has pixels with white color saturated indicating the basalt occurrence and hence, the mines. The figure also shows other areas identified as basalt that were not mapped by GPS, indicating the presence of other mines.

The advantage using this technique over conventional classification techniques is that it has greater control over the results. Based on the image "rule", filters can be applied over the pixels with the highest probability of belong the study class, whereas in the other classification techniques, the pixels are classified according to a range of values, which are similar.

Classification with reference spectra extracted directly from images always tend to have better results because factors such as lighting conditions, particles and aerosols, the spectral influence of other targets are already associated with the image and consequently the spectral curve. Due to the small size of basalt areas (usually less than one pixel at 15m ASTER) spectral signature of reference cannot be extracted in the ASTER image because the same had not totally pure pixels.

5. Conclusions

The results showed that ASTER images can be employed for mineral characterization, in the study case, the basalt extracted from amethysts mining.

The algorithm MaxVer produced satisfactory results. The main problem was the mixing (error) between Shadow, Soils and Basalt classes.

The SAM technique has achieved better results than MaxVer, being able to identify the pixels with greater spectral similarity. Even areas where basalt occurrence was small, sometimes lower than one pixel, the technique could identify the basalt spectral influence, of course, with a lower similarity value.

The forest native present beside the mines has great influence on the pattern detection process and extraction of reference spectra. Therefore, to generate reference spectra that are more pure and reliable, large areas should be chosen, where the vegetation and shadow influence are smaller.

The low spectral contrast of basalt in VNIR/SWIR region (Figure 3.1) is a factor that influences the classifications results. Due to the small intensity of diagnostic features, basalt may be easily mix with other classes like shadow and soils. A better approach to study this kind of rock may be employing emissivity data on thermal infrared region (8 - 12 μ m). In this region, the quartz, a mineral that compounds basalts rocks, has more intensity spectral features, also known as restrahlen bands, while other classes like soils, vegetation and shaded areas tend to behave like a gray body.

References

- [1] Abrams, M., and Hook, S.J., 2002: *Aster User Handbook: Advanced Spaceborne Thermal Emission and Reflection Radiometer*. USA: NASA/Jet Propulsion Laboratory, California Institute of Technology. 2; 135.
- [2] Boardman, J.W., Kruse, F.A., and Green, R.O., 1995: *Mapping Target Signatures via Partial Unmixing of AVIRIS Data*. In: Summaries, Fifth JPL Airborne Earth Science Workshop. JPL Publication 95-1. 1; 23-26.
- [3] Breunig, F.M., 2008: *Dados De Reflectância E Emissividade Do Sensor ASTER/Terra Aplicados Ao Estudo De Solos Quartzosos*. Dissertação de Mestrado. INPE.
- [4] Carvalho junior, O, A., Carvalho, A.P.F., Meneses, P.R., Guimarães, R.F., and Martins, E.S. *Análise de imagens hiperespectrais pelo método Multiple Endmember Spectral mixture Analysis (MESMA) em depósito supergênico de níquel*. Revista Brasileira de Geociências. 2003. 33 (1).
- [5] Chen, J.Y., and Reed, I.S. *A Detection Algorithm for Optical Targets in Clutter*. IEEE Trans. on Aerosp. Electron. Syst. 1987. AES-23 (1).
- [6] Clark, R.N., and Swayze, G.A., 1995: *Mapping Minerals, Amorphous Materials, Environmental Materials, Vegetation, Water, Ice, and Snow, and Other Materials: The USGS Tricorder Algorithm*. In Summaries of the Fifth Annual JPL Airborne Earth Science Workshop, JPL Publication 95-1. 39-40.
- [7] Crósta, A.P., 1993: *Processamento Digital de Imagens de Sensoriamento Remoto*, Campinas, SP, UNICAMP, ed. rev.
- [8] Ducart, D.F., Crósta, A.P., and Souza Filho, C.R. *Mapeamento De Alteração Hidrotermal No Distrito De Los Menucos, Argentina, Por Meio De Imagens Multiespectrais ASTER*. In: Simp. Bras. de Sens. Rem., Goiânia, INPE/SELASR. 2005. 12; 4057-4064.
- [9] ENVI User Guide, 2009: *Atmospheric Correction Module: QUAC and FLAASH User's Guide*. Version 4.7.
- [10] ERSDAC (Earth Remote Sensing Data Analysis Center), 2003: *The Crosstalk Correction Software User's Guide*. 21.
- [11] Galvão, L.S., Almeida-Filho R., and Ícaro, V. *Spectral Discrimination of Hydrothermally Altered Materials using ASTER Short-Wave Infrared Bands: Evaluation in a Tropical Savannah Environment*. International Journal of Applied Earth Observation and Geoinformation. 2005. 7; 107-114.
- [12] Gao, B.C., Hiedebrecht, K.B., and Goetz, A.F.H. *Derivation of Scaled Surface Reflectance are from AVIRIS Data*. Remote Sensing of Environment. 1993. 44; 165-178.

- [13] Goetz, A.F.H. *The Spectral Image Processing System (SIPS) - Interactive Visualization and Analysis of Imaging Spectrometer Data: Remote Sensing of Environment*. Special Issue on AVIRIS. May-June 1993. 44; 145-163.
- [14] Goetz, A.F.H., Vane, G., Solomon, J.E., and Rock, B.N. *Imaging Spectrometry for Earth Remote Sensing*. Science. 1985. 228; 1147-1153.
- [15] Goetz, A.F.H. *The Spectral Image Processing System (SIPS) – Interactive Visualization and Analysis of Imaging Spectrometer Data*. Remote Sensing Environment. 1993. 44; 145-163.
- [16] Green, A.A., Bermam, M., Switzer, P., and Craig, M.D. *A Transformation for Ordering Multispectral Data in Terms of Image Quality with Implications for Noise Removal*. IEEE Transactions on Geosciences and Remote Sensing. 1988. 26 (1) 65-74.
- [17] Harsanyi, J.C., and Chang, C. *Hyperspectral Image Classification and Dimensionality Reduction: an Orthogonal Subspace Projection Approach*. IEEE Transactions on Geosciences and Remote Sensing. 1994. 32; 779-785.
- [18] Iwasaki, A., and Tonooka, H. *Validation of a Crosstalk Correction Algorithm for ASTER/SIWR*. IEEE Transactions on Geosciences and Remote Sensing. 2005. 43 (12) 2747-2751.
- [19] Kalinowski, A., and Oliver, S. 2004: *ASTER Mineral Index Processing Manual*. Ed. Geosciences Australia.
- [20] Kruse, F.A., Lefkof, A.B., Boardman, J.W., Heiedbrechet, K.B., Shapiro, A.T., Barloon, P.J., and Goetz, A.F.H. *The Spectral Image Processing System (SIPS) – Interactive Visualization and Analysis of Imaging Spectrometer Data*. Remote Sensing Environment. 1993. 44; 145-163.
- [21] Matthew, M.W., S.M. Adler-Golden, A. Berk, S.C. Richtsmeier, R.Y. Levine, L.S. Bernstein, P.K. Acharya, G.P. Anderson, G.W. Felde, M.P. Hoke, A. Ratkowski, H.H. Burke, R.D. Kaiser, and D.P. Miller. *Status of Atmospheric Correction Using a MODTRAN4-based Algorithm*. SPIE Proceedings, Algorithms for Multispectral, Hyperspectral, and Ultraspectral Imagery VI. 2000. 4049; 199-207.
- [22] Nunes, G.M., Souza Filho, C.R., and Ferreira, L.G. *Caracterização De Fisionomias Vegetais Em Área De Floresta Tropical Através De Análises Espectrais Em Dados E Produtos Do Sensor ASTER*, In: Simp. Bras. de Sens. Rem., Florianópolis, INPE. 2007. 13; 6497-6504.
- [23] Nunes, G.M., 2008: *Sensoriamento Remoto Aplicado Na Análise Da Cobertura Vegetal Das Reservas De Desenvolvimento Sustentável Amanã E Mamirauá*. Tese de Doutorado, IAG-Unicamp.
- [24] Richards, J.A., 1993: *Remote Sensing Digital Image Analysis*. Springer, Heidelberg, New York.
- [25] Smith, M.O., and Adams, J.B. *Interpretation of AIS Images of Cuprites, Nevada, Using Constrains of Spectral Mixtures*. In: Airborne Imaging Spectrometer Data Analysis Workshop. Pasadena, CA. Proceedings, JPL Publ. 1985. 85-41, 62-68.
- [26] Schowengerdt, R.A., 2007: *Remote Sensing: Models and Methods for Image Processing*. Third Edition. Academic Press. 509.

- [27] Souza Filho, C.R., Tápia, C.H., Crósta, A.P., and Xavier, R.P., 2003: *Infrared Spectroscopy and ASTER Imagery Analysis of Hidrotermal Alteration Zones at the Quellaveco Porphyry-Cooper Deposit, Southern Peru*. In: Proceedings of the American Society of Photogrammetry and Remote Sensing (ASPRS), Annual Conference – Technology: Converging at the Top of the World. 1-12.
- [28] SULSOFT, Guia do ENVI em Português. Disponível em: <<http://www.envi.com.br>>. Acesso em: 06/07/2013.
- [29] Van der Meer, F., 2000: *Imaging Spectrometry Geological Applications*. In: The Encyclopedia of Analytical Chemistry, Meyers R.A. (Ed.), John Wiley & Sons Ltd., Sussex, U.K. 8601-8638.
- [30] Vicente, L.E., 2007: *Caracterização De Sistemas Ambientais Tropicais Complexos Utilizando Análise Sistêmica E Classificação Hiperespectral De Dados Do Sensor ASTER (Advanced Spaceborne Thermal Emission And Reflection Radiometer)*. Tese de Doutorado, IAG-Unicamp.